Monatshefte für Chemie 137, 529–543 (2006)
DOI 10.1007/s00706-006-0462-8

Monatshefte für Chemie
Chemical Monthly
Printed in Austria

Invited Review

Small-Angle X-Ray Scattering to Characterize Nanostructures in Inorganic and Hybrid Materials Chemistry[#]

Herwig Peterlik[1,*] and **Peter Fratzl**[2]

[1] Institute of Materials Physics, University of Vienna, A-1090 Vienna, Austria
[2] Department of Biomaterials, Max-Planck-Institute of Colloids and Interfaces, D-14424 Potsdam-Golm, Germany

Received December 22, 2005; accepted (revised) February 6, 2006
Published online May 5, 2006

Summary. With the improved control of the nanostructure and the handling of multicomponent systems in sol–gel chemistry, the research interest in this field increased significantly in the past decade. For the characterization of the nanostructure of inorganic–organic hybrid materials, small-angle X-ray scattering has proven to be one of the most important techniques. By using X-rays from synchrotron radiation sources, even the structural development during processing can be followed *in-situ*. This short note reviews some analytical evaluation procedures used to study hybrid materials. While numerical simulation tools are nowadays available to obtain detailed fits of scattering curves, the use of analytical models is still very useful if the evaluation and interpretation of the obtained parameters is straightforward.

Keywords. X-Ray structure determination; Clusters; Nanostructures.

Introduction

In the past decade hybrid inorganic–organic materials attracted increasing scientific interest. Sol–gel chemistry not only offers the possibility to develop new types of ceramics or glasses, but also to incorporate organic moieties in inorganic materials due to the mild reaction conditions [1]. Together with the improved control of the mesostructure and the handling of a multicomponent system, an enormous variety in combining the different components allows to deliberately tailor materials with improved or new properties. In the past decade, this has stimulated research in areas that include catalysis and sensors [2], coatings [3], membranes

* Corresponding author. E-mail: herwig.peterlik@univie.ac.at
[#] Dedicated to Prof. *Ulrich Schubert* on the occasion of his 60th anniversary

[4], nanoreactors [5], or in electronic applications [6]. Modern chemistry enables the control of size, shape surface area, surface, and interfacial properties as well as the mutual arrangement and morphology from completely disordered to completely ordered states of matter in the range between 2 and 500 nm [7]. The development of large, low density silica monoliths, which can additionally be produced with a hierarchical organisation of macro- and periodically oriented mesopores [8], further extends the potential field of application to structural materials.

Small-angle X-ray scattering (SAXS) is one of the most powerful methods to characterize the structure of materials at the nanoscale [9, 10]. Scanning of specimens enables the determination of the nanostructure in the laboratory with a position resolution of 50 microns, which is of particular importance for hierarchical structures such as the biological hybrid material bone [11]. The further development of focussed X-rays from third generation synchrotron radiation sources improves the position resolution in real space down to the submicron range (*e.g.* 100 nm X-ray beam using a wave-guide structure [12]). The high intensity of X-ray beams in synchrotron radiation sources additionally allows to follow the formation and evolution of the network during sol–gel processing with a time resolution in the range of minutes or even seconds [13].

Due to the enormous amount of scientific literature published in this research field in the last years, an extensive overview is nearly impossible and would exceed the length restrictions of a journal article. Thus, we concentrate in this work on describing a number of simple analytical evaluation procedures which have been used to determine the nanostructure in hybrid inorganic–organic materials using SAXS. In general, computer simulation techniques coupled to numerical fitting procedures have proven to be very powerful in describing small-angle scattering from complex matter. The three-dimensional shape and domain structure was determined by *ab initio* modelling from one-dimensional SAXS patterns [14, 15] and successfully applied, *e.g.* for biological macromolecules [16, 17]. The advantage of analytical evaluation procedures is that they can easily be compared to the large amount of data available in the literature, if the interpretation of the obtained structural parameters is straightforward. The intention here is not to give a full account of such analytical procedures or review all evaluation methods published in literature, but to focus on some very useful simple procedures and their physical background.

SAXS in Inorganic and Hybrid Materials

Polydisperse Systems

Polydisperse systems consist of basic structural units covering an extremely wide range of size distributions. An example for such systems are sol–gel derived aerogels, which exhibit a highly porous and foam-like structure at the nanometer scale (Fig. 1). Typical features of the structural composition at this scale are visualized in Fig. 2: particles build up a network of branched clusters up to a certain length scale, above which continuum-like behavior is observed. In the following, we focus here on a silica/titania system originating from a single-source precursor. A precise description of the chemical composition and processing may be found in Ref. [18].

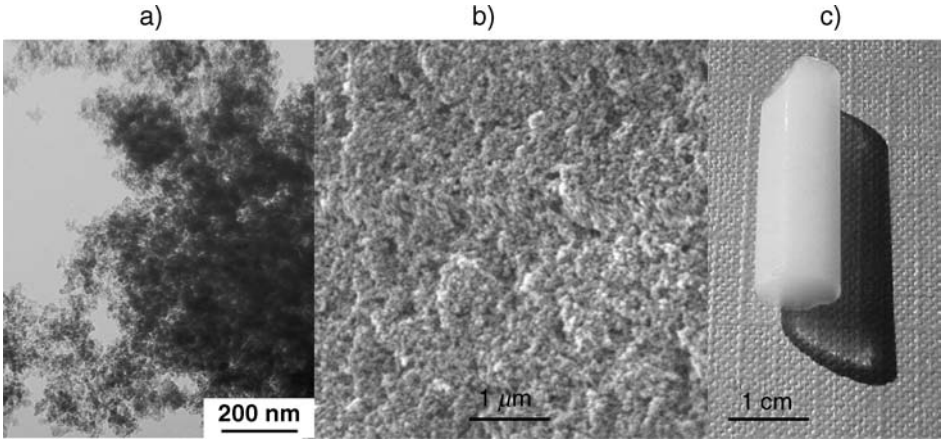

Fig. 1. Structure of an aerogel at different length scales: a) foam-like structure at the nanometer scale, b) coarse structure at the micrometer scale, c) monolith at the centimeter scale

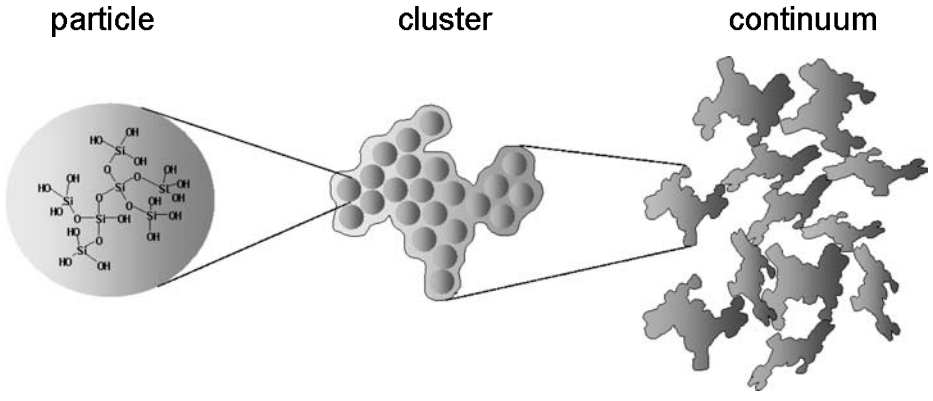

Fig. 2. Scheme of the structural features of a network built up of particles

For a material, consisting of a collection of identical particles and for example forming a network, the scattering intensity can be written as Eq. (1) [19, 20].

$$I(q) = I_0 N {V_0}^2 \Phi(q) S(q) P(q) \tag{1}$$

Here I_0 is a constant containing experimental parameters such as beam intensity, phase contrast between the two phases, and additional variables due to the setup of the experiment. N is the number of primary particles, V_0 is the volume of the primary particle, $S(q)$ the structure factor describing the packing of the primary particles, $P(q)$ the form factor of the particle, and $\Phi(q)$ a factor to correct for concentration effects due to close packing. Usually, this equation has to be supplemented by the background scattering BGR from the specimen or the equipment as in Eq. (2) [20].

$$\frac{I(q)}{I_0} = BGR + N {V_0}^2 \Phi(q) S(q) P(q) \tag{2}$$

For the volume, a widely used choice is to assume particles of spherical shape with a radius r, $V_0 = 4\pi r^3/3$ [16]. The form factor for spherical particles is well-known as Eq. (3) [21, 22].

$$P(q) = (3(\sin(qr) - qr\cos(qr))/(qr)^3)^2 \tag{3}$$

The strong oscillations of the function given by Eq. (3) are usually smeared out to a varying degree depending on the size distribution of the particles. For a very wide size-distribution, a convenient approximation is the *Debye* function (Eq. (4)) [19, 20] which tends to become unity for $q \to 0$ and towards $9/2(qr)^{-4}$ for large q, which matches the average large q decay of the exact solution for the form factor of a single sphere [21, 22].

$$P(q) = \left(1 + \sqrt{2}q^2r^2/3\right)^{-2} \tag{4}$$

However, the decay of Eq. (4) is smooth, because the oscillations of the exact solution for monodisperse particles are smeared out. The curvature of the form factor at small values of q is also quite different for the *Debye* approximation, that is, $P(q) \approx 1 - (2\sqrt{2}/3)q^2r^2$ instead of $P(q) \approx 1 - q^2r^2/5$ for the exact solution for monodisperse particles. The largest deviation is around $q\ r = 2.4$, where the *Debye* approximation underestimates the exact solution by about a factor of 4 (Fig. 3). This curvature generally depends on the particle size distribution and in this sense, the *Debye* approximation corresponds to an extremely wide size distribution.

A simple expression can be obtained for the structure factor $S(q)$ by assuming individual scatterers with a spatial distribution according to a power-law correlation function and a cut-off distance ξ. The parameter ξ is a correlation length, above which the material exhibits macroscopic density and continuum-like, but not fractal behavior [23, 24]. This correlation length can then be related to the radius of gyration r_g of the clusters by Eq. (5) [24].

$$\xi = \sqrt{2D(D+1)}r_g \tag{5}$$

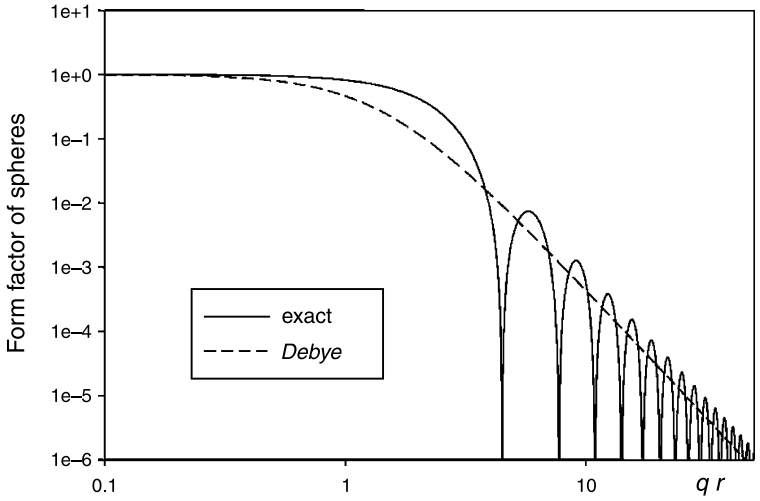

Fig. 3. Comparison of the form factor for monodisperse spheres, Eq. (3), to the *Debye* approximation, Eq. (4)

D is the fractal dimension of the aggregate of particles. For monodisperse spheres, $r_g = \sqrt{5/3}r$ and in the *Debye* approximation, $r_g = 8^{1/4}r$. The choice of a correlation length (the cluster size) together with individual scatterers, which obey a size distribution according to a power-law, enables an analytical solution, Eq. (6), for the structure factor by *Fourier* transformation [23], where C is a constant.

$$S(q) = 1 + \frac{C\Gamma(D-1)\xi^D}{q\xi}\left(1 + \frac{1}{(q\xi)^2}\right)^{(1-D)/2} \mathrm{Sin}\left((D-1)\arctan(q\xi)\right) \quad (6)$$

If the cluster size exceeds the accessible range of the equipment, Eq. (6) may further be simplified to Eq. (7).

$$S(q) = 1 + \frac{C\Gamma(D-1)\xi^D}{q\xi}\mathrm{Sin}\left((D-1)\pi/2\right) \quad \text{for } \xi \to \text{Infinity} \quad (7)$$

There are some minor differences in the prefactors of Eq. (6) in literature [19, 20, 23–25]. In principle, NV_0 is proportional to the total volume of the particles and $1 + C\Gamma(D-1)\xi^D$ to the number of particles per aggregate, derived from the limiting behavior towards $q \to 0$ [25].

Figure 4a shows a scheme of the scattering curve of an aerogel network, with the continuum range for $1/q > \xi$, the network range with a decrease of the scattering intensity $I(q) \propto q^{-D}$ for a mass fractal and $I(q) \propto q^{-(6-D)}$ for a surface fractal with fractal dimension D, and the surface range, where the intensity decays with $I(q) \propto q^{-4}$ due to a sharp interface between two phases (known as *Porod*'s law [26]). In Fig. 4b, an example of a mixed silica–titania aerogel is shown together with the fit of the curve according to Eq. (2).

With such approximations, the evaluation of SAXS data enables the determination of the particle and the cluster size as well as the fractal dimension. One should

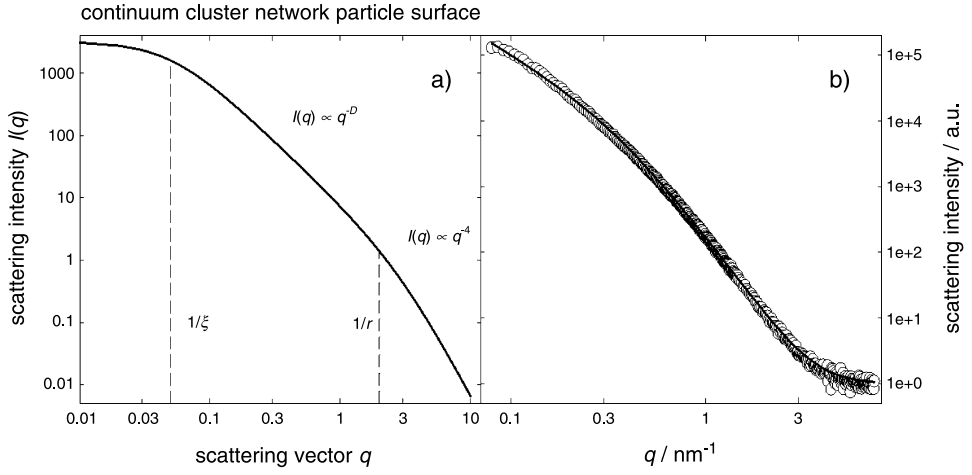

Fig. 4. a) Schematic of the scattering diagram of an aerogel built up of a network of particles; the chosen dimensionless parameters were particle size $r = 0.5$, cluster size $\xi = 20$, and fractal dimension $D = 2$; three ranges are visible, the continuum range $1/q > \xi$, the network range $\xi > 1/q > r$, and the surface range of the particle $r > 1/q$; b) experimental data of a calcined silica–titania aerogel with background normalized to 1 and fit parameters $r = 3.9$ nm, cluster size $\xi = 50$ nm, and fractal dimension $D = 1.9$

be careful in the interpretation, if the fractal range is small so that a linear decrease of the intensity is hard to identify. It should also be kept in mind, however, that there are considerable approximations in these analytical expressions. Computer simulations of particle aggregation are now available [27], which allow direct predictions of scattering functions and much more reliable comparisons. Dense networks exhibit a higher value of the fractal dimension than open networks. The fractal dimension allows to draw conclusions on the specific form of aggregation: Computer simulations have shown that particle-cluster or hierarchical cluster–cluster aggregation together with diffusion-limited, ballistic, or reaction-limited aggregation processes lead to distinguishable values in the fractal dimension [28].

Clustered Material with Short-Range Order

New types of hybrid inorganic–organic materials have been produced by introducing nanosized inorganic building blocks, which maintain their integrity, into organic polymers. The covalent bonding of these clusters to the organic polymer chains is achieved by using clusters substituted by polymerizable organic groups as precursors in polymerization reactions [29]. Phase separation frequently occurs in such systems during preparation due to difficulties in controlling the size and shape of the fillers inside the organic medium [30]. The presence of covalent bonds or strong molecular interactions, *e.g*. hydrogen bonding, is one of the possible strategies to tackle the separation effect [30]. To exclude a possible phase separation as well as to determine the distance of clusters and their amount of order, SAXS turned out to be a useful method. As an example, we focus in the following to an inorganic–organic hybrid polymer, *i.e*. the organic polymer polystyrene was reinforced with a metal oxo cluster, a schematic being shown in Fig. 5. The scattering intensity of pure polystrene and polystyrene doped with different amounts of Zr6-clusters (0.24 mol% and 0.87 mol%) is depicted in Fig. 6. Two features are visible: The peak at large q-values originates from the short-range order of Zr6-clusters and increases with increasing molar ratio of clusters, and the second intensity maximum at low q-values being due to the polymer is nearly unaffected from the amount of clusters.

For extremely dilute systems, the *Guinier* approximation (Eq. (8)) allows the determination of the cluster size from the radius of gyration r_g [21, 22] from the

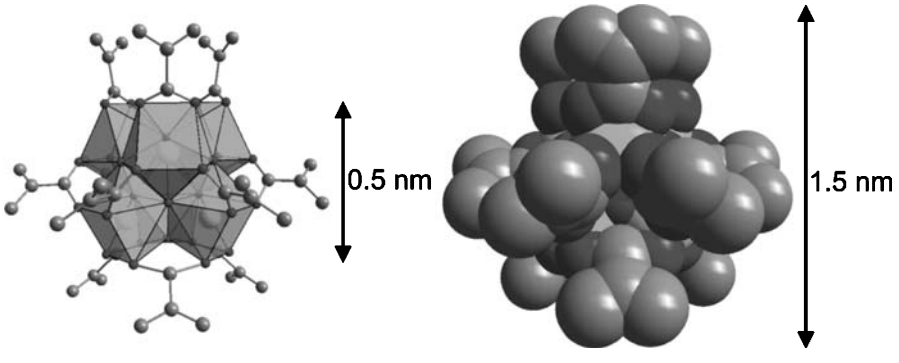

Fig. 5. Schematic presentation of a molecular structure of typical metal oxo clusters

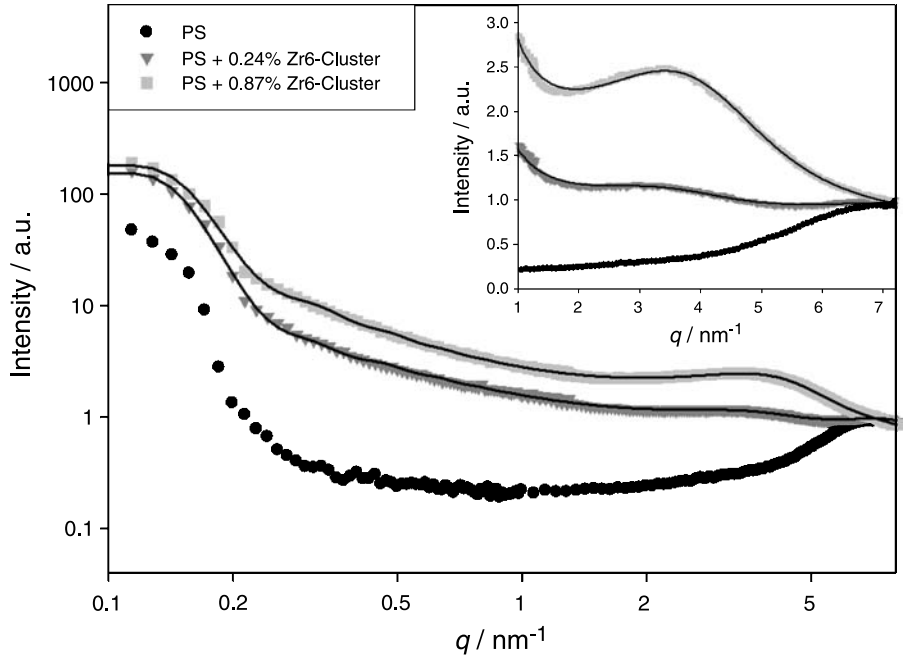

Fig. 6. Scattering intensity of polystyrene (black symbols) with different amount of Zr6-cluster (0.24 mol%, dark grey symbols; 0.87 mol%, light grey symbols); the small insert in the figure shows the data in linear scale to visualize the Zr6-cluster peak; the lines are fits according to Eq. (12)

slope in a diagram of the logarithmic intensity *vs*. the square of the scattering vector towards small q.

$$\ln\left(I(q)\right) \approx \ln\left(I(q)\right) - \frac{q^2 r_g^2}{3} \tag{8}$$

This approach should be taken with caution due to several reasons: Interparticle interference may influence the initial part of the scattering curve, which can be eliminated by measuring with different concentrations and extrapolating to infinite dilution. Possible aggregation of particles may also lead to distortion of the scattering curve. For the evaluation, only q-values $q \leq 2\pi/r_g$ should be taken into account. Figure 7 shows the *Guinier* evaluation according to Eq. (8) for the data as in Fig. 6. The size of spherical clusters is related to the radius of gyration by (Eq. (9)) [21, 22].

$$r = \sqrt{5/3}\, r_g \tag{9}$$

An important information is the mean distance d of the clusters. In a first approximation, it can be derived from the maximum of the peak $q_{\max}$ in the scattering curve by the simple relation of Eq. (10).

$$d = \frac{2\pi}{q_{\max}} \tag{10}$$

Strictly speaking, this relation is only correct for a periodic arrangement of particles with a spacing d, where the maximum corresponds to a sharp *Bragg* peak.

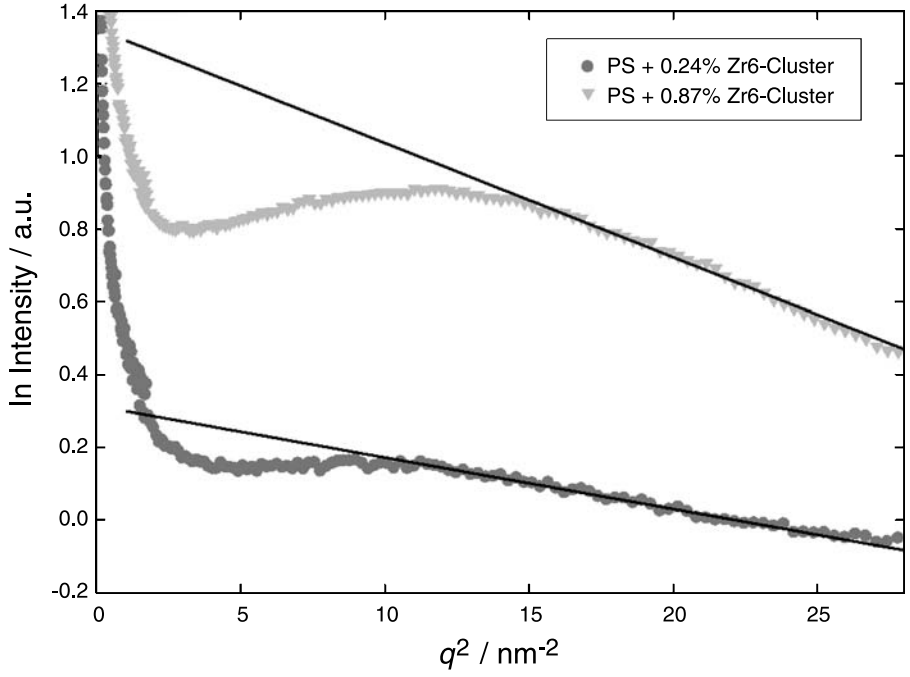

Fig. 7. Evaluation from the *Guinier* approximation for polystyrene doped with Zr6-clusters (0.24 mol%, dark grey symbols; 0.87 mol%, light grey symbols); the lines are fits according to Eq. (8)

If there is only a short-range order in the arrangement of the particles, the peak is broadened and the peak position may also shift considerably, so that Eq. (10) can only be used for a very rough order-of-magnitude estimate of d.

The evaluation according to Eq. (10) results in a decrease of the cluster distance from 1.84 to 1.71 nm and an increase of the radius of gyration, Eq. (8), from 0.21 to 0.31 nm with an increasing molar ratio of Zr6-clusters. A more elaborate evaluation uses the approach proposed by *Beaucage* [31]. It composes a scattering curve of two functions, one being based on *Guinier*'s law and the other on the structurally limited power law (Eq. (11)).

$$I(q) = g \exp\left(-q^2 r_g^2/3\right) + b\left(\left(\operatorname{erf}\left(q r_g/\sqrt{6}\right)\right)^3/q\right)^p \tag{11}$$

Here g and b are fit parameters depending on the volume of the scatterers, the scattering contrast, and the experimental equipment, erf is the error function, and p the exponent of the power law. For multiple structural levels, one has to use two or more of these functions, where the indices in Eq. (12) denote the different radii of gyration. This is only valid in the dilute limit, where no interference of the particles takes place. For a high content of particles, Eq. (12) was supplemented by the interference function $\Phi(q, k, d)$ describing the concentration effect due to a dense packing [30, 31]. The correlation distance of the respective scatterers is denoted by d, k is a packing factor, $k = 8V_0/V_1$, with V_0 the volume of the primary cluster and $V_1 = V/N$ the average volume provided to each subunit, and V the total volume provided to N particles. The interference function is here applied to both distributions, whereas in literature it was taken into account only for the second

distribution, as the maximum of the first one was not in the accessible range of the X-ray equipment [30].

$$\Phi(q,k,d) = \frac{1}{1+k\theta(q,d)} \qquad (12)$$
$$\theta(q,d) = 3\,\frac{\sin(qd) - qd\cos(qd)}{(qd)^3}$$

and

$$\begin{aligned} I(q) = {} & g_1 \exp(-q^2 {r_{g1}}^2/3)\Phi(q,k_1,d_1) + b_1 \exp(-q^2 {r_{g2}}^2/3) \\ & \times((\mathrm{erf}(qr_{g1}/\sqrt{6}))^3/q)^{p_1}\Phi(q,k_1,d_1) + g_2 \exp(-q^2 {r_{g2}}^2/3)\Phi(q,k_2,d_2) \\ & + b_2 \exp(-q^2 {r_{g2}}^2/3)((\mathrm{erf}(qr_{g2}/\sqrt{6}))^3/q)^{p_2}\Phi(q,k_2,d_2) \end{aligned}$$

This approach was successfully applied to describe the structural change as well as the development of the mechanical properties of a polymer doped with titanium-oxo-clusters [30]. The main problem in the use of Eq. (12) is the high number of fit parameters, which complicates the reliability of the fitted parameters considerably. It is recommended to fit the scattering curve in an iterative way, first only at high q-values for one distribution and then only at low q-values for the other to find appropriate starting values for the final fit. A further simplification is to reduce the number of fit parameters, *e.g.* to set $p_2 = 4$ for particles with a smooth surface [30]. Fitting can be performed by an appropriate software such as Mathematica. As an example, the result from the fit to polystyrene doped with different amounts of zirconia clusters is shown in Fig. 6 as solid lines, the numerical values of the fit are found in Table 1. From these data, only the packing density increases, whereas all other parameters are nearly unchanged. Thus, this example shows that different interpretations may arise when using different models to describe experimental data.

In some cases, more than two maxima were observed in the scattering curve at low q-values, which could both be attributed to two characteristic cluster distances, as in the pure undoped material these peaks were not found. This was interpreted as an arrangement of clusters in a discotic structure (Fig. 8) [29, 32]. The shorter distance d_1 would then correspond to the inter-cluster distance within piles of discs and the longer distance d_2 to the distance between clusters of neighbouring piles, which is visualized in Fig. 8. To distinguish between the different kinds of clusters and to ease the interpretation of SAXS-data, additional chemical information from the reactivity of the components and from other experimental characterization techniques such as TEM proved to be very useful [29, 32].

Table 1. Fit values from Eq. (12) to the data shown in Fig. 6; with increasing cluster proportion, the packing density k_2 increases, whereas other parameters are nearly unchanged

	r_{g1}/nm	p_1	k_1	d_1/nm	r_{g2}/nm	k_2	d_2/nm
PS + 0.24% Zr	16.4	1.33	3.07	39.5	0.406	1.32	1.38
PS + 0.87% Zr	16.1	1.70	2.85	38.1	0.399	1.73	1.29

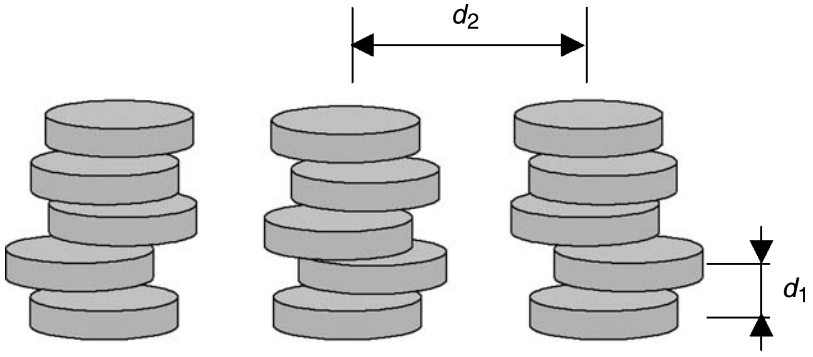

Fig. 8. An arrangement of discs may also result in more than two characteristic distances, resulting in two maxima in the scattering intensities [25, 28]

Mesostructured Materials with Long-Range Order

Mesostructured materials with long-range order exhibit *Bragg* reflections. However, due to the large dimension of the basic structural units, such reflections are visible only in the small-angle X-ray scattering range. Figure 9 shows an example for a material with an ordered structure at the mesoscale, based on a liquid templating approach from the ethylene glycol route.

The evaluation usually follows the basic evaluation procedures in diffraction [2, 8, 33, 34]. The distance of the basic structural units is derived from Eq. (10) and the type of ordering (frequently hexagonal, lamellar, or cubic) from the position of the respective reflections. The size of the coherent scattering region is frequently estimated from the full-width at half-maximum Δq of the first and usually most intense reflection, known as *Scherrer*'s formula (Eq. (13)) [35].

$$L = K\frac{2\pi}{\Delta q} \tag{13}$$

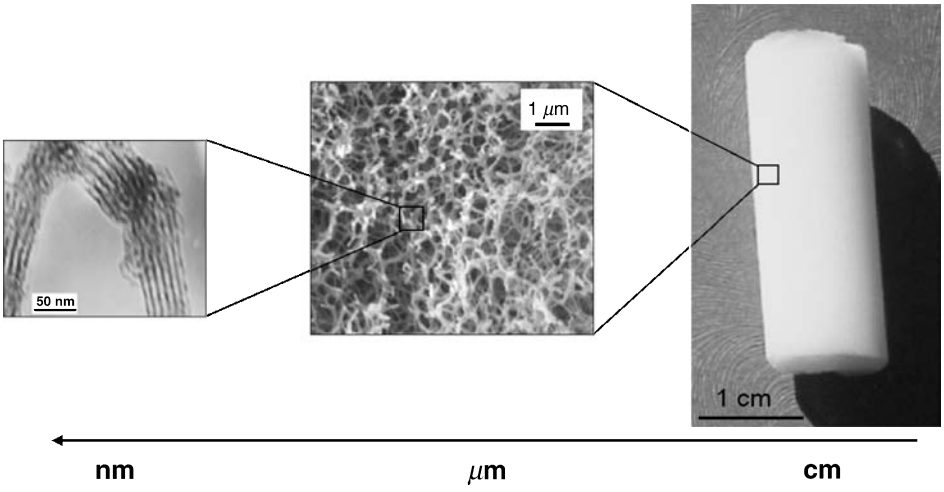

Fig. 9. Mesostructured material with a hierarchical organization and a periodic ordered structure at the nanoscale [29]

Here L is the crystallite size and K a constant close to 1 depending on the shape of the crystallite. For the application of Eq. (13), the width of the detector/equipment resolution has to be significantly smaller than the width of the *Bragg* reflection, which is not generally the case in particular in small-angle X-ray scattering. Otherwise, a deconvolution of the scattering signal is necessary. The experimental determination of the resolution of the equipment requires a crystal of infinite size with a lattice constant in the same range as the specimens to be measured, which is in general not easily available. A possible material coming close to these requirements is rat tail tendon in the direction of the reflections of the D-period.

Advanced evaluation procedures were developed to determine the size and distance distributions as well as the orientation of the lamellae of preferably oriented nanocomposite films [36, 37] and the structural parameters of weakly ordered membrane systems by line-shape analysis [38]. However, extensive experience in scattering theory is required. Also, the description of the dimension of a three-phase systems with a hydrophobic, a micro-, and a mesoporous domain is available [39]. For the sake of simplicity, we restrict ourselves here only to a two-phase system (material/no material). The intensity ratio of the reflections of hexagonally arranged long and elongated cylinders allows the simultaneous determination of the distance and the wall thickness of the cylinders by making use of the following three assumptions: a) the cylinders are infinitely long with radius r_c, which results in the form factor (Eq. (14)) [21].

$$P(q) = \frac{4\pi r_c^2}{q}\left(\frac{J_1(qr_c)}{qr_c}\right)^2 \tag{14}$$

b) The cylinders are arranged in a hexagonal lattice with a certain size distribution, which can be described by a *Gaussian* or *Lorentzian* function, and c) the half-width of the reflection increases with increasing number due to the higher lattice distortion for the higher orders of the reflections. A complete description additionally has to take into account the intensity decrease and the line broadening due to the *Lorentz*-factor, the *Debye-Waller* factor, and the limited size of the lattice. To obtain the experimental scattering intensity $I_{exp}(q)$, the theoretical intensity $I_{th}(q)$ is convolved with the resolution function of the equipment, Eq. (15).

$$I_{exp}(q) = I_{th}(q) \otimes res(q) \tag{15}$$

A numerically faster procedure is the use of the convolution theorem and *Fourier* transforms (Eq. (16)).

$$I_{exp}(q) = F^{-1}(F(I_{th}(q))F(res(q))) \tag{16}$$

The intensity ratio of the first reflections was used to determine the diameter and the wall thickness of hexagonally arranged structural units and was compared to the results from *BET* measurements [8]. Figure 10 shows experimental SAXS-data for materials with two different wall thicknesses and comparable distance of the hexagonally arranged cylindrical basic units. In the insert of Fig. 10, an enlargement is depicted for better visualization of the two higher reflections. For the smaller wall thickness, the second reflection is higher than the third, whereas the opposite is the case for a larger wall thickness. A calculation according to Eq. (15)

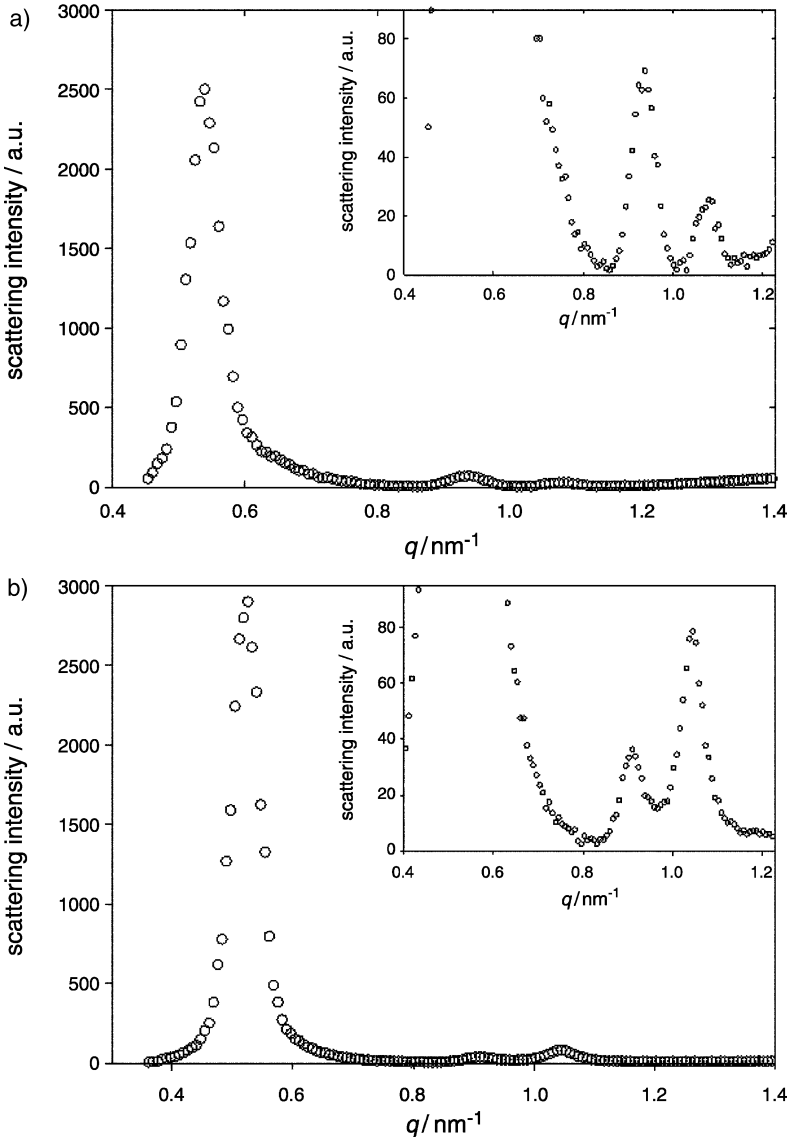

Fig. 10. SAXS data for a mesoporous silica monolith with different wall thicknesses: a) cylinder–cylinder distance 13.9 nm and wall thickness 2.8 nm with the second reflection exhibiting a higher intensity than the third, b) cylinder–cylinder distance 13.9 nm and wall thickness 4.5 nm with the opposite behavior

is presented in Fig. 11, which visualizes the strong effect of a change in the wall thickness on the intensities of the higher reflections.

Time-Resolved Characterization of Structures

The high intensity of X-ray beams from synchrotron radiation sources allows to improve the position and/or time resolution in comparison to laboratory equipments by orders of magnitude. This enables the direct observation of the formation of the network of inorganic–organic materials during processing [18, 25] or

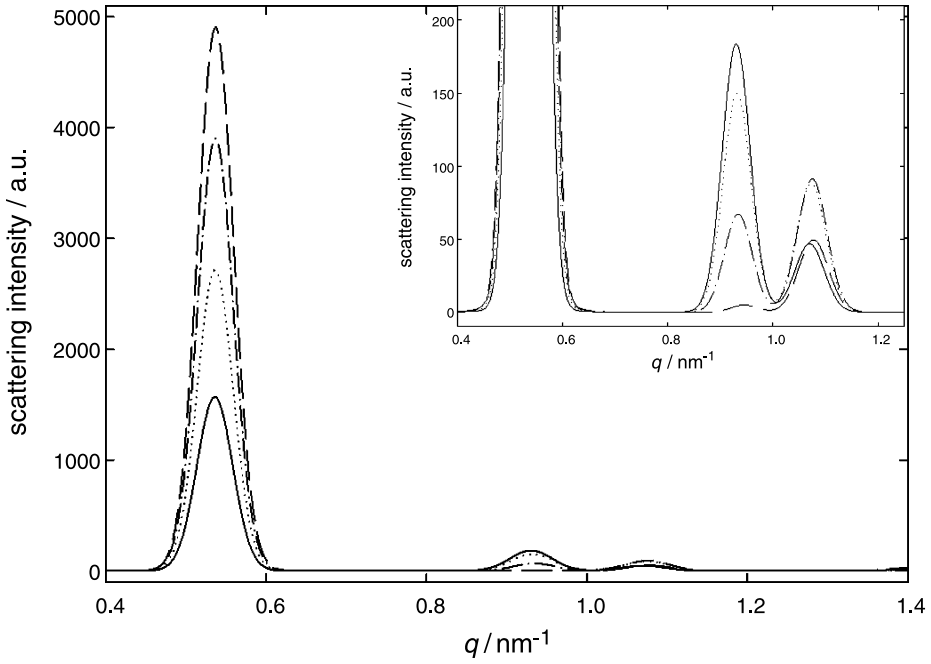

Fig. 11. Simulation of the intensity of the reflections with a cylinder–cylinder distance of 13.5 nm and a varying wall thickness: 2 nm, solid line; 3 nm, dotted line; 4 nm, dashed-dotted line; 5 nm, dashed line; the insert is an enlargement for better visualization of the relative change of the intensity of the higher reflections

thermal treatment [40], nucleation and growth of silica colloids [41], the study of *in situ* phase transformations [42], or *in situ* development of ordered cell wall structures in mesoporous hybrid materials [43]. Figure 12 shows as an example

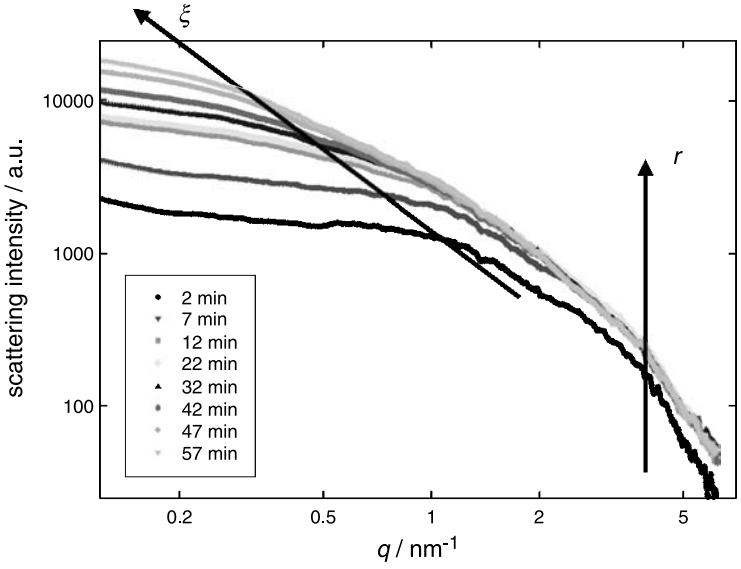

Fig. 12. Intensity increase of a gel prepared from a silica/titania single-source precursor during gelation measured *in-situ* using X-rays from a synchrotron radiation source; the particle size r (right arrow) remains nearly constant, whereas the cluster size ξ (left arrow) increases continuously in real space

the development of the network structure of a gel, prepared from a silica/titania single-source precursor, during the gelation process. The growth of the cluster size is visualized by the left arrow, whereas the particle size remains nearly unchanged (right arrow). A numerical evaluation of the cluster and the particle size as well as the fractal dimension was performed by using Eq. (2) [18, 25].

X-Rays were also successfully applied to investigate the change in the reflection of a long-range ordered mesoporous material during processing [44]. Even the supercritical drying procedure with high pressure and elevated temperatures can be followed [44] by the use of a specially designed pressure cell equipped with diamond windows [45].

Conclusion

SAXS is a powerful method to characterize the nanostructure of inorganic–organic hybrid materials. Numerous evaluation procedures were developed and applied to polydisperse systems as well as systems with short or long range order. In a short review, some of the most useful methods are presented, which should help scientists from materials chemistry or chemical engineering in the application of these evaluation techniques and in the comprehension of the background from materials physics.

Acknowledgements

We are grateful to *U. Schubert*, *N. Hüsing*, *D. Brandhuber*, *V. Torma*, and *R. Kogler* for the long-time interdisciplinary cooperation and for many helpful discussions.

References

[1] Schubert U, Hüsing N, Lorenz A (1995) Chem Mater **7**: 2010
[2] Lu YF, Ganguli R, Drewien CA, Anderson MT, Brinker CJ, Gong WL, Guo YX, Soyez H, Dunn B, Huang MH, Zink JI (1997) Nature **389**: 364
[3] Caruso RA, Antonietti M (2001) Chem Mater **13**: 3272
[4] Liu C, Martin CR (1991) Nature **325**: 50
[5] Stein A, Melde BJ, Schroden RC (2002) Adv Mater **12**: 1403
[6] Fendler JH (2001) Chem Mater **13**: 3196
[7] Antonietti M, Ozin GA (2004) Chem Eur J **10**: 28
[8] Brandhuber D, Peterlik H, Hüsing N (2005) J Mater Chem **15**: 3896
[9] Kostorz G (1991) J Appl Cryst **24**: 444
[10] Fratzl P (2003) J Appl Cryst **36**: 397
[11] Rinnerthaler S, Roschger P, Jakob HF, Nader A, Klaushofer K, Fratzl P (1999) Calc Tiss Int **64**: 422
[12] Lagomarsino S, Jark W, DiFonzo S, Cedola A, Mueller B, Engstrom P, Riekel C (1996) J Appl Phys **79**: 4471
[13] Grosso D, Babonneau F, Sanchez C, Soler-Illia GJDA, Crepaldi EL, Albouy PA, Amenitsch H, Balkenende AR, Brunet-Bruneau A (2003) J Sol-Gel Sci Techn **26**: 561
[14] Volkov VV, Svergun DI (2003) J Appl Cryst **36**: 860
[15] Konarev PV, Volkov VV, Sokolova AV, Koch MHJ, Svergun DI (2003) J Appl Cryst **36**: 1277
[16] Svergun DI, Koch MHJ (2003) Rep Progr Phys **66**: 1735
[17] Svergun DI, Koch MHJ (2002) Curr Opin Struc Biol **12**: 654

[18] Torma V, Peterlik H, Bauer U, Rupp W, Hüsing N, Bernstorff S, Steinhart M, Goerigk G, Schubert U (2005) Chem Mater **17**: 3146
[19] Emmerling A, Petricevic R, Beck A, Wang P, Scheller H, Fricke J (1995) J Non-Cryst Solids **185**: 240
[20] Hüsing N, Schubert U, Mezei R, Fratzl P, Riegel B, Kiefer W, Kohler D, Mader W (1999) Chem Mater **11**: 451
[21] Guinier A, Fournet G (1955) Small-Angle Scattering of X-rays, Chapman & Hall, London
[22] Feigin LA, Svergun DI (1987) Structure Analysis by Small-Angle X-ray and Neutron Scattering, Plenum Press, New York
[23] Freltoft T, Kjems JK, Sinha SK (1986) Phys Rev B **33**: 269
[24] Teixera J (1988) J Appl Cryst **21**: 781
[25] Krakovsky I, Urakawa H, Kajiwara K, Kohjiya S (1998) J Non-Cryst Solids **231**: 31
[26] Porod G (1951) Kolloid Z **124**: 83
[27] Svergun D (2005) http://www.embl-hamburg.de/ExternalInfo/Research/Sax/software.html
[28] Meakin P (1999) J Sol-Gel Techn **15**: 97
[29] Moraru B, Hüsing N, Kickelbick G, Schubert U, Fratzl P, Peterlik H (2003) Chem Mater **14**: 2732
[30] Trabelsi S, Janke A, Hässler R, Zafeiropulous NE, Fornasieri G, Bocchini S, Rozes L, Stamm M, Gerard JF, Sanchez C (2005) Macromolecules **38**: 6068
[31] Beaucage G (1996) J Appl Cryst **29**: 134
[32] Torma V, Hüsing N, Peterlik H, Schubert U (2004) Compte Rendu Chimie **7**: 495
[33] Brandhuber D, Torma V, Raab C, Peterlik H, Kulak A, Hüsing N (2005) Chem Mater **17**: 4262
[34] Guinier A (1952) X-ray crystallographic technology, Hilger and Watts Ltd., London
[35] Patterson AL (1939) Phys Rev **56**: 978
[36] Ruland W, Smarsly B (2004) J Appl Cryst **37**: 575
[37] Ruland W, Smarsly B (2005) J Appl Cryst **38**: 78
[38] Pabst G, Koschuch R, Pozo-Navas B, Rappolt M, Lohner K, Laggner P (2003) J Appl Cryst **36**: 1378
[39] Smarsly B, Polarz S, Antonietti M (2001) J Phys Chem B **105**: 10473
[40] Grosso D, Soler-Illia GJDA, Crepaldi EL, Cagnol F, Sinturel C, Bourgeois A, Brunet-Bruneau A, Amenitsch H, Albouy PA, Sanchez C (2003) Chem Mater **15**: 4562
[41] Pontoni D, Narayanan T, Rennie AR (2002) Langmuir **18**: 56
[42] Grosso D, Babonneau F, Soler-Illia GJDA, Albouy PA, Amenitsch H (2002) Chem Comm **7**: 748
[43] Morell J, Teixeira CV, Cornelius M, Rebbin V, Tiemann M, Amenitsch H, Fröba M, Lindén M (2004) Chem Mater **16**: 5564
[44] Hüsing N, Brandhuber D, Raab C, Torma V, Peterlik H, Steinhart M, Kriechbaum M, Bernstorff S (2003) Elettra Highlights 2002–2003: 32
[45] Pressl K, Kriechbaum M, Steinhart M, Laggner P (1997) Rev Sci Instr **68**: 4588